# Radially expanding transglial calcium waves in the intact cerebellum

Tycho M. Hoogland[a,b,1,2], Bernd Kuhn[a,b,1,2], Werner Göbel[c], Wenying Huang[a], Junichi Nakai[d,3], Fritjof Helmchen[c], Jane Flint[a], and Samuel S.-H. Wang[a,b,2]

[a]Department of Molecular Biology and [b]Princeton Neuroscience Institute, Princeton University, Lewis Thomas Laboratory, Washington Road, Princeton, NJ 08544; [c]Brain Research Institute, University of Zürich, Winterthurerstrasse 190, 8057 Zürich, Switzerland; and [d]Laboratory for Memory and Learning, RIKEN Brain Science Institute, 2-1, Hirosawa, Wako-shi, Saitama 351-0198, Japan

Edited by Charles F. Stevens, The Salk Institute for Biological Studies, La Jolla, CA, and approved January 14, 2009 (received for review September 16, 2008)

**Multicellular glial calcium waves may locally regulate neural activity or brain energetics. Here, we report a diffusion-driven astrocytic signal in the normal, intact brain that spans many astrocytic processes in a confined volume without fully encompassing any one cell. By using 2-photon microscopy in rodent cerebellar cortex labeled with fluorescent indicator dyes or the calcium-sensor protein G-CaMP2, we discovered spontaneous calcium waves that filled approximately ellipsoidal domains of Bergmann glia processes. Waves spread in 3 dimensions at a speed of 4–11 $\mu$m/s to a diameter of ≈50 $\mu$m, slowed during expansion, and were reversibly blocked by P2 receptor antagonists. Consistent with the hypothesis that ATP acts as a diffusible trigger of calcium release waves, local ejection of ATP triggered P2 receptor-mediated waves that were refractory to repeated activation. Transglial waves represent a means for purinergic signals to act with local specificity to modulate activity or energetics in local neural circuits.**

astrocytes | Bergmann glia | in vivo | 2-photon microscopy | G-CaMP2

Like most eukaryotic cell types, astrocytes mobilize calcium from internal stores. Astrocytic calcium signals can also spread from cell to cell, as demonstrated in a variety of explanted central nervous system tissues, including cell culture (1–3), retina (4), and neocortical brain slices (5).

Advances in optical imaging methods have allowed astrocytic calcium signals to be imaged in vivo. Astrocytic signals occur spontaneously in the neocortex (6, 7) and can be evoked by somatosensory (8) and visual stimuli (9), highlighting their potential significance for normal function. In all cases, the observed signals have occurred in well-defined populations of a few astrocytes at once.

Under some circumstances, calcium signals also spread in a wave-like fashion across many glial cells. In the retina, focal stimulation can trigger spreading astrocytic waves (4). Spreading astrocytic waves can be triggered by focal electrical stimulation in brain slices (10) and by ATP release in culture (3, 11). Glial waves have been observed in radial glia in the developing neocortex (12) and in models of spreading depression (13–15).

We examined astrocytic signaling in the cerebellum in vivo, which has not been characterized previously. We used in vivo 2-photon microscopy in combination with either bolus loading of calcium indicators or expression of the genetically encoded calcium sensor protein G-CaMP2 targeted to Bergmann glia (BG), the astrocytes of the molecular layer (ML). In brain slices, BG mobilize calcium in response to a number of neurotransmitters (16, 17) and can generate subcellular domains of calcium release in response to synaptic stimulation via activation of purinergic receptors (18, 19).

Here, we report that BG calcium release can be organized into highly symmetric waves. We characterize these waves in 3 dimensions and show that they form near-ellipsoidal domains that span dozens of processes. Wave generation and intercellular propagation require the local release of a small purine followed by its diffusional spread.

## Results

**Spontaneous Calcium Waves in Bergmann Glia in Vivo.** To measure glial calcium signals in vivo we performed 2-photon laser scanning microscopy on cerebellar folia crus I and II in anesthetized rats and mice. We first used multicell bolus loading (MCBL) (20) of calcium indicators in rat cerebellar cortex (21). By using fluo-5F/AM ($K_D$ = 1.0 $\mu$M), visible structures in the ML were brightly labeled glial processes and faintly labeled interneurons (Fig. 1*A*). Processes were identified as BG palisades by their orientation along the parallel fiber (PF) axis and by the fact that they arose from numerous appendages sprouting from larger main processes (22) (Fig. 1*A*, supporting information (SI) Movie S1). This labeling pattern was confirmed by photoconversion of fluo-4 and fluo-5F to electron-dense products for examination by transmission electron microscopy (23). Live imaging revealed signals in subcellular processes and an unusual widespread type of spontaneous calcium signal in the form of spreading transglial waves. Waves initiated at a center point, then expanded radially to encompass multiple BG stem processes and their appendages (Fig. 1*B*, Movie S2). In total we analyzed 108 spontaneous calcium wave events in 22 rats, and 23 spontaneous calcium wave events in 11 mice.

**Three-Dimensional Characterization of Transglial Calcium Waves.** The duration of calcium signals, defined as the interval during which the mean fluorescence change reached or exceeded 10% of the peak value, was 11 ± 5 s (range, 3–22 s) in rats, comparable to signals previously observed in vitro (18). Within the normal *xy*-imaging plane signals filled approximately elliptical domains with a mean area of 3,500 ± 2,800 $\mu$m$^2$ (Fig. 1*C*, Table S1). The maximum extent was reached within an expansion time of 4.2 ± 2.1 s.

The elliptical appearance of domains spanning multiple BG suggested that they were mediated by a diffusible extracellular signal emanating from a single source. Consistent with diffusion, the wavefront velocity decreased from near-center values by ≈60% at a distance of 40 $\mu$m (Fig. 1*D*). The apparent diffusion coefficient $D_{app}$ of the expanding area $A$, calculated by using the relation $D_{app} = A/4t$, was 165 ± 11 $\mu$m$^2$/s (mean ± SEM). Diffusion-mediated spread should be anisotropic because extracellular diffusion in the ML is ≈1.4-fold faster in the PF axis than in the perpendicular direction (24). Consistent with this, transglial do-

Author contributions: T.M.H., B.K., W.G., F.H., and S.S.-H.W. designed research; T.M.H., B.K., and W.G. performed research; T.M.H., B.K., W.G., W.H., J.N., F.H., and J.F. contributed new reagents/analytic tools; T.M.H. and B.K. analyzed data; and T.M.H., B.K., F.H., and S.S.-H.W. wrote the paper.

The authors declare no conflict of interest.

This article is a PNAS Direct Submission.

[1]T.M.H. and B.K. contributed equally to this work.

[2]To whom correspondence may be addressed. E-mail: hoogland@princeton.edu, bkuhn@princeton.edu, or sswang@princeton.edu.

[3]Present address: Saitama University Brain Science Institute, 255 Shimo-Okubo, Sakura-ku, Saitama City, Saitama 338-8570, Japan.

This article contains supporting information online at www.pnas.org/cgi/content/full/0809269106/DCSupplemental.

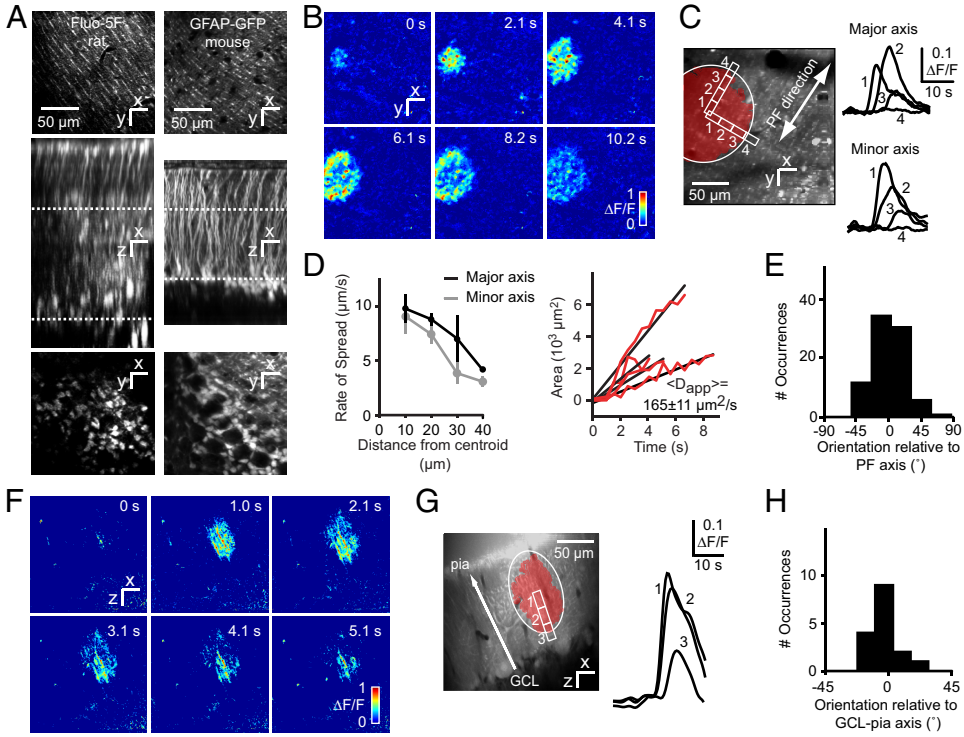


**Fig. 1.** Transglial calcium waves in the cerebellar cortex in vivo. (*A*) Staining patterns of the cerebellar cortex bolus-loaded with fluo-5F/AM (rat) or expressing GFP under the glial cell-specific GFAP promoter (mouse). (*Top*) Optical sections acquired in the molecular layer [ML, locations indicated by the upper dotted lines (*Middle*)] show a distinct striate pattern matching lateral protrusions from stem processes of Bergmann glia (BG). (*Middle*) Maximal side projection showing similarity between fluo-5F/AM labeling and GFAP-GFP expression. (*Bottom*) Optical sections taken from the Purkinje cell layer, with BG somata arranged around Purkinje cells. (*B*) Spontaneous radial wave measured in the ML. (*C*) Putative stem processes and side branches from BG show calcium increases with a time course typical of glial signals. (*D*) (*Left*) Wavefront slowing with distance from the initiation site. (*Right*) Linear rate of increase of wave area, with an average apparent diffusion constant $D_{app}$ = 165 $\mu m^2/s$. Data are shown for 4 waves. (*E*) Distribution of wave orientation relative to the parallel fiber (PF) axis. (*F*) Radial wave in ML measured in an *xz* parasagittal plane orthogonal to the surface of the cerebellum. (*G*) Wave orientation along the axis of BG stem processes. (*H*) Distribution of wave orientation relative to the pia–Purkinje cell axis.

mains had an average major-to-minor axis ratio of 1.3 ± 0.2, major and minor axis lengths of 37 ± 13 and 29 ± 12 $\mu$m, and were oriented along the PF axis (angle of deviation $\theta = 2 \pm 22°$; Fig. 1*E*).

To characterize spread of transglial waves in the third dimension, in a second set of experiments we used "arbitrary plane imaging" (25). Rat cerebellar cortex was bolus-loaded with OGB-1/AM and scanned in an *xz* parasagittal plane, parallel to Purkinje cell (PC) dendritic arbors and perpendicular to the PF axis (Fig. 1*F*, Movie S3). Waves formed elliptical domains in the parasagittal plane (Fig. 1*G*; Table S1). Domains were oriented along the pia-granule cell layer axis (deviation $\theta = 4 \pm 12°$, Fig. 1*H*) with a major-to-minor axis ratio of 1.5 ± 0.2 (Fig. 1*G*). Anisotropy coincides with the presence of BG stem processes running in the *z* direction, suggesting that signals may spread or be amplified within individual BG.

**Spread of Calcium Waves Through Bergmann Glia.** To visualize transglial waves more clearly in BG we used the nonreplicating adenovirus AdEasy-1 (26) to express the calcium-sensitive fluorescent protein G-CaMP2. When injected into the mouse cerebellar cortex in vivo, this adenovirus infected only glial cells, consistent with in vitro observations (27). Reconstruction and calcium measurements were possible to a depth of 230 $\mu$m in the 2 main astrocyte populations, BG (Fig. 2*A*) and velate astrocytes in the granule cell layer. By varying the amount and depth of virus injection and the time after infection we obtained infection patterns ranging from sparse labeling of individual BG (Fig. 2*A*, Movie S4) to complete labeling in a region >250 $\mu$m wide. Between 1 and 25 days postinfection no dead cells or changes in tissue appearance or BG morphology (compared with GFP-GFAP mice) were observed.

Radially expanding calcium waves were observed throughout the ML (Fig. 2*B*, Movie S5), with fluorescence changes of up to 93% above baseline in individual processes. Domains were oriented along the PF axis (Fig. 2 *C* and *D*) and had a $D_{app}$ of 152 ± 17 $\mu m^2/s$ (mean ± SEM), indistinguishable from rat ($P = 0.84$, 2-tailed *t* test). Compared with MCBL-loaded rat cerebellum, domains were smaller (major and minor axis lengths of 25 ± 5 and 19 ± 4 $\mu$m, $P < 0.001$, 2-tailed *t* test) and briefer (6 ± 2 s, $P < 0.001$, 2-tailed *t* test), perhaps reflecting the high cooperativity of G-CaMP2 for calcium (Hill coefficient = 3.8). In addition, velate astrocytes also showed transglial waves (5 events, 3 mice; Movie S6) at a depth of up to 100 $\mu$m below the Purkinje cell layer, indicating that they are triggered in the granular layer. Velate cell waves had an expansion time of 2.5 ± 0.4 s, lasted 10.4 ± 3.3 s, and had a diameter of 49 ± 12 $\mu$m.

We estimated the number of BG cells and processes encompassed by the domain of a single transglial wave. Reconstructed image stacks from GFAP-GFP mice had a density of one BG per 84 ± 16 $\mu m^2$ in the *xy* plane. Thus, an average domain of 1,500 $\mu m^2$ overlies 1,500/84 = 18 BG cells, and assuming 4 processes per BG, 72 ± 28 processes. However, the processes in a domain come from an even larger number of cells because unlike neocortical astrocytes (28), BG interdigitate with one another in the ML. In tissue that expressed G-CaMP2 sparsely (Fig. 2*A*, Movie S4), processes from individual BG spanned regions measuring 40 ± 10 $\mu$m across parasagittally and 19 ± 3 $\mu$m across in the parallel fiber direction (3 BG from 3 mice). Thus, processes may originate from BG somata both directly underlying the domain and in a surrounding annulus 20 $\mu$m thick parasagittally and 9.5 $\mu$m longitudinally. The total number of BG somata contained in

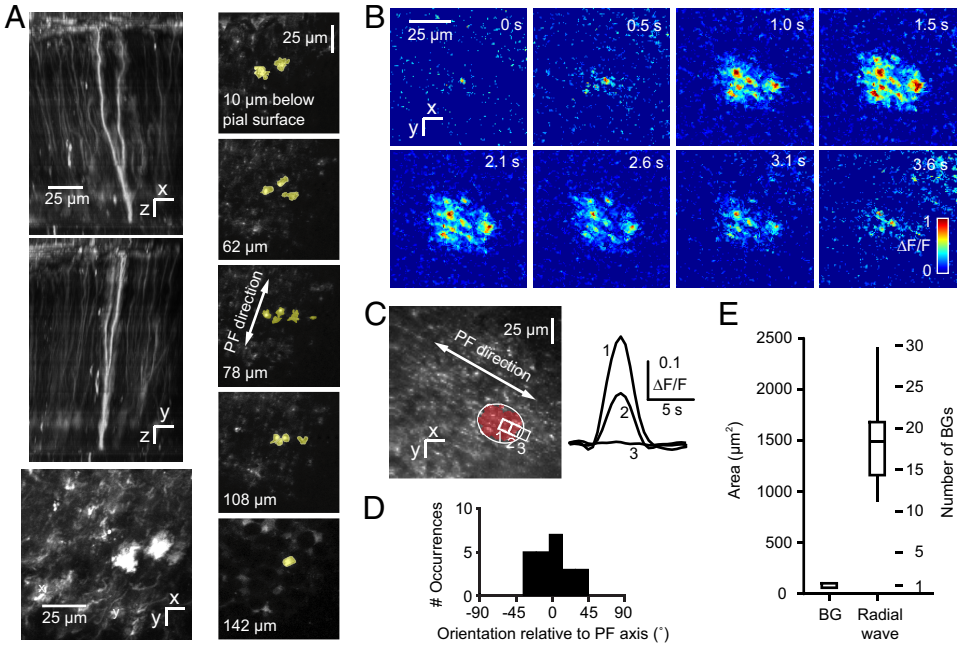


**Fig. 2.** Transglial calcium waves in BG imaged with G-CaMP2 in vivo. (*A*) (*Left*) Maximum brightness side projections of DsRed expression after infection of the mouse cerebellum with an adenovirus carrying the sequence for the fusion protein G-CaMP2_DsRed. (*Bottom Left*) Molecular layer section showing BG processes. (*Right*) *x*–*y* sections at different levels below pia mater show extent and branching of a single BG. (*B*) Radial wave measured with G-CaMP2 in the molecular layer. (*C*) A transglial wave domain. (*D*) Orientation of domains relative to the parallel fiber axis. (*E*) Distribution of domain sizes relative to a single BG.

this larger effective domain is 51 ± 11 cells, all of which potentially contribute to the transglial wave.

**Spontaneous Subcellular Glial Calcium Signals.** In addition to waves we also observed subcellular calcium transients in G-CaMP2-expressing BG that resembled microdomains previously described in brain slices (29). In *xy* scans of BG processes these transients were 5.5 ± 1.6 μm wide and lasted 2.4 ± 0.8 s (18 events in 5 mice, Fig. S1 *A* and *B*). In velate astrocytes the transients occurred mainly in processes, had a diameter of 7.6 ± 1.9 μm, and lasted 2.6 ± 0.8 s (13 events, 4 mice; Fig. S1*C*). Subcellular events were also detected in MCBL experiments but the assignment to specific cellular structures was not possible because of the low contrast and lack of cell-type specificity.

**Transglial Calcium Waves Recur in the Same Location.** The expanding dynamics of waves suggested that they were triggered at discrete origination sites. In search of repeated wave origination from the same site we monitored fields of view in the ML for 14 to 96 min. Movies contained 2 to 30 events each (Fig. 3*A*) that often overlapped in space (Fig. 3*B*). If waves originated at random locations, the squared center-to-center distance of pairs of overlapping events should be uniformly distributed (Fig. 3*C*, gray histogram). In contrast, for actual overlapping pairs, squared distances were skewed toward short distances (Fig. 3*C*, red histogram; different from uniform distribution, $P < 0.01$, Kolmogorov–Smirnov test), consistent with the existence of wave-triggering foci.

Extended monitoring also allowed us to test whether waves were triggered by laser illumination (30). Events appeared at a uniform rate of 0.40 ± 0.13 waves per minute of observation (Fig. 3*D*; rate not correlated with observation time, $P = 0.3$, n.s., 2-tailed *t* test), suggesting that events are not illumination-induced. Waves could also initiate outside the FOV and sometimes began before the start of imaging. Calcium waves were observed under all types of anesthesia used: urethane, ketamine/xylazine, and isoflurane (Table S1 and Table S2). Thus, transglial calcium waves occur spontaneously under a variety of conditions.

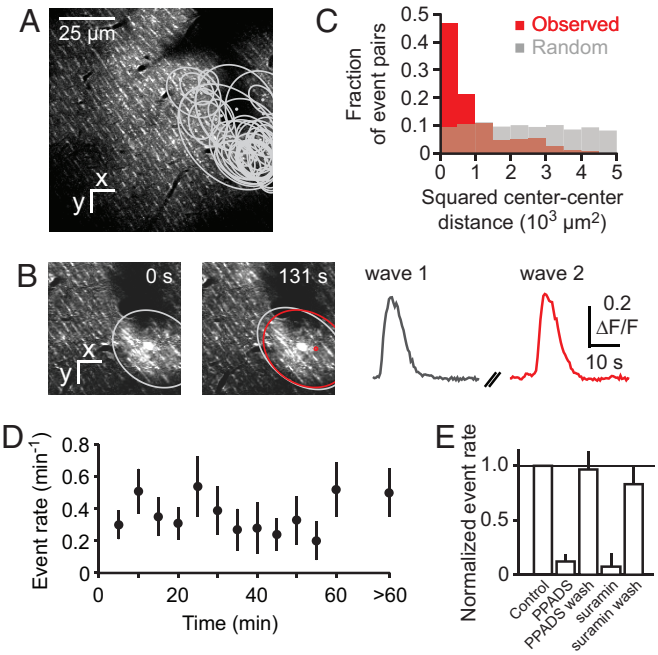


**Fig. 3.** Recurrence of transglial calcium waves at the same location. (*A*) Locations of all transglial waves recorded in a field of view from rat tissue bolus-loaded with fluo-5F. (*B*) Two example events. (*C*) The distribution of squared center-to-center distances between different events (red) differs from random expectations (Monte Carlo model; gray). (*D*) Constancy of the rate of transglial wave events during long-term imaging, averaged >8 fields of view. (*E*) The rate of spontaneous transglial calcium waves during topical application of PPADS (500 μM) and suramin (1 mM) and after washout (wash), normalized to control.

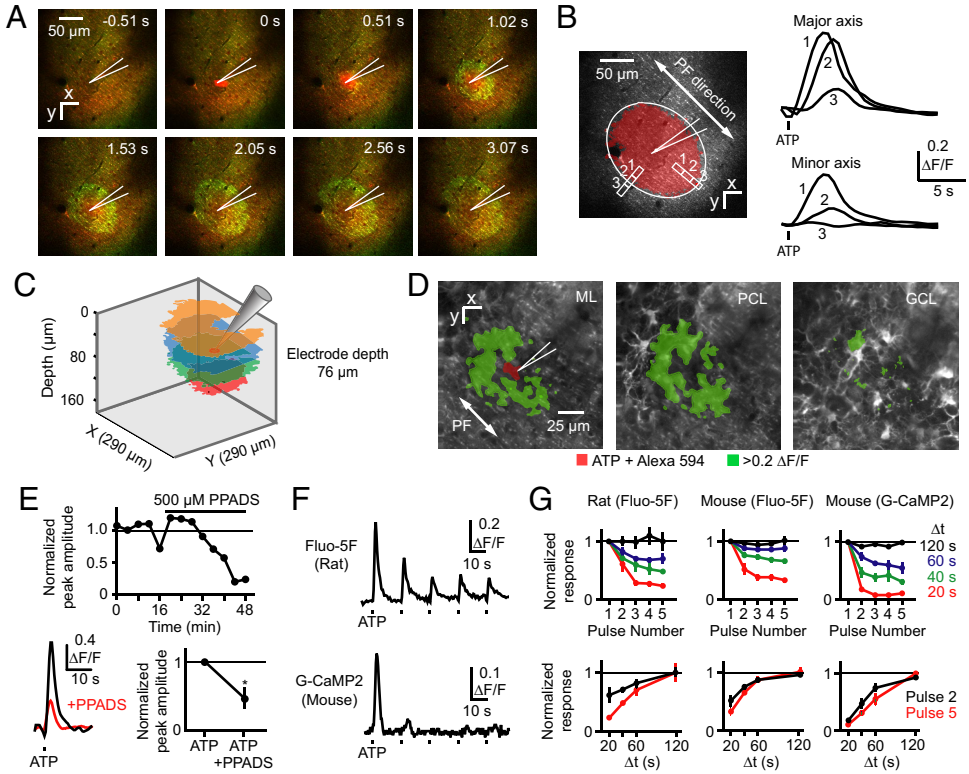


**Fig. 4.** ATP-triggered transglial calcium waves in vivo. (*A*) A transglial calcium wave evoked by ejection of ATP (pipette concentration: 1 mM, 10 ms, 0.07 bar) into the molecular layer. Green, Fluo-5F calcium signal; red, Alexa 594 and SR101. (*B*) Elliptical domain oriented along the PF axis in an ATP-triggered wave. (*C*) Waves triggered in rat cerebellar cortex at different imaging depths after ATP ejection at the same depth. (*D*) Activation of velate astrocytes in the granule cell layer after ATP ejection in lower third of the molecular layer, imaged by using G-CaMP2. (*E*) Reduction of ATP-triggered transglial signals by the P2 antagonist PPADS. (*F*) Decrease in successive calcium responses after repeated application of ATP. (*G*) Dependence of response amplitude after 5 pulses of ATP injected at different time intervals.

**Spontaneous Transglial Calcium Waves Are Reversibly Blocked by P2 Receptor Antagonists.** BG express a variety of G protein-coupled receptors that couple to calcium release from intracellular stores (17, 31), including P2Y receptors, which are activated by ATP (16, 18, 19). To test whether spontaneous transglial waves rely on a purinergic receptor-dependent mechanism, we imaged transglial waves in rats before, during, and after surface application of the P2 receptor antagonists PPADS (500 $\mu$M, Fig. S2), or suramin (1 mM). The rate of spontaneous events as measured with Fluo-5F was significantly reduced to 12 $\pm$ 6% of control for PPADS ($n = 4$) and 7 $\pm$ 12% for suramin ($n = 3$), respectively (Fig. 3*E*; $P < 0.01$, 2-tailed t tests). After PPADS and suramin were carefully rinsed off the brain surface with saline, the rate fully recovered to 96 $\pm$ 17% and 83 $\pm$ 17% of control (Fig. 3*E*, PPADS, $P < 0.01$, suramin, $P < 0.05$, 2-tailed tests).

**Local ATP Injection Triggers Radially Expanding Transglial Waves.** The ability of purinergic receptor antagonists to block spontaneous waves suggests that local release of ATP could trigger calcium waves. To test this possibility we pressure-ejected ATP from a pipette placed in the ML of rats and mice loaded with fluo-5F/AM or mice expressing G-CaMP2. In all cases, ATP evoked spreading calcium waves similar to spontaneous waves (Fig. 4*A*, Movie S7; Table S1, Table S3). Filled elliptical domains (Fig. 4*B*) had similar orientation (rat Fluo-5F, $P = 0.8$; mouse Fluo-5F, $P = 0.7$; mouse G-CaMP2, $P = 0.9$, 2-tailed $t$ test) and major-to-minor axis ratio as spontaneous waves (rat Fluo-5F, $P = 0.7$; mouse Fluo-5F, $P = 0.3$; mouse G-CaMP2, $P = 0.7$; 2-tailed $t$ test). No calcium waves were triggered by pressure ejection of saline (3 mice). ATP-triggered waves filled regions that were larger and more variable than spontaneous waves (19,000 $\pm$ 8,000 $\mu$m$^2$, range 7,800–30,600 $\mu$m$^2$, 8 events in 4 rats; $P < 0.05$, 2-tailed $t$ test). $D_{app}$ was similarly variable (700–3,000 $\mu$m$^2$/s). $D_{app}$ was correlated with the size of the responding region (rank correlation, +1.0), suggesting that signaling mechanisms may have been saturated by the amount of ATP injected or that pressure ejection introduced a nondiffusive component to the wave spread.

To examine the 3-dimensional geometry of ATP-triggered waves, ATP was injected repeatedly at one location and calcium changes were imaged at different depths. Waves were visible at a range of scan depths, indicating an overall ellipsoidal geometry (Fig. 4*C*). ATP injection at the pial surface and in the molecular and Purkinje cell layers could trigger waves. Injection in the lower third of the ML spread to underlying Purkinje cell somata (Movie S8) and velate astrocytes (Fig. 4*D*). Thus, all of the depths at which waves originate and propagate are sensitive to ATP.

We used ATP to further probe the properties of spreading calcium events. As was observed for spontaneous events, application of PPADS (500 $\mu$M) to the brain surface reduced the amplitude of ATP-triggered signals by 53 $\pm$ 30% ($P < 0.05$, $n = 3$) from control (Fig. 4*E*), consistent with a P2 receptor-dependent mechanism. P2 receptor activation triggers calcium release from internal stores (19, 32), which after activation can be refractory for tens of seconds as refilling occurs (33). We delivered 5 successive ATP injections at different-spaced time intervals (Fig. 4 *F* and *G*). At the shortest interval tested, 20 s, the fifth response to ATP was reduced to 23 $\pm$ 4% (rat, fluo-5F, $n = 4$), 33 $\pm$ 4% (mouse, fluo-5F, $n = 4$), and 11 $\pm$ 2% (mouse, G-CaMP2, $n = 4$) of the size of the first response. At 120-s intervals the amplitude of the fifth response was undiminished at 100 $\pm$ 16% (rat, fluo-5F), 100 $\pm$ 7% (mouse, fluo-5F), and 99 $\pm$ 3% (mouse, G-CaMP2) of the first response. Responses recovered to half the size of the first response in an

estimated 27 ± 9 s (rat, fluo-5F), 30 ± 6 s (mouse, fluo-5F), and 37 ± 4 s (mouse, G-CaMP2), consistent with refilling times for internal stores. These results are consistent with a mechanism in which point-like release of ATP acts on P2 receptors to trigger transcellular calcium release waves.

## Discussion

This work represents the first demonstration in the intact brain of intercellular calcium waves triggered by purinergic mechanisms. The occurrence of spontaneous calcium waves encompassing multiple BG processes within a defined volume represents a means for normal tissue to generate a regional signal.

**Subcellular and Spreading Events.** Our observation of spontaneous calcium signals in individual BG processes echoes previous findings in other brain regions in vivo, where signals tend not to spread between neighbors, are unresponsive to purinergic receptor blockers, and have functionally nonoverlapping domains (9, 34).

Subcellular signals coexisted in the same tissue with more widespread signals spanning dozens of processes in well-delimited, approximately ellipsoidal spaces. Resolution and assignment of signals to BG cellular processes was made possible by the use of G-CaMP2. G-CaMP2 also provided a means of obtaining measurements without acute introduction of a dye-containing electrode, which could damage tissue. The fact that a less invasive approach yielded repeated ellipsoidal waves indicates that they are not pathological, unlike spreading depression, another wave-like phenomenon seen in neocortical (14, 15) and cerebellar (13) astrocytes that differs by being independent of purinergic receptor activation (13), having higher speeds (>15 $\mu$m/s), and a spatial range of millimeters. Waves recurred in the same location, but were not restricted to functional domains, because waves with spatially segregated initiation centers could overlap. Wave domains were seen throughout the molecular layer, with their major axis in the transverse plane oriented along the PF axis, whereas the long axis in the sagittal plane follows the direction of the main processes of BG. These features suggest that ellipsoidal waves can be driven repeatedly throughout the molecular layer by purine release events. Recent reports indicate that in awake animals, BG signals may occur repeatedly in larger spatial domains than the current report.[†]

**Origin and Mechanism of Expanding Transglial Waves.** Whether the purinergic triggering signal arises from neurons or glia is currently unknown. Astrocytes can release ATP in a point-like fashion (11), opening the possibility that BG or parts thereof could activate neighboring BG. Such a feedback step could account for why the apparent diffusion coefficient for spontaneous waves was somewhat slower than the estimated diffusion constant of ATP (200–400 $\mu m^2/s$) (35), raising the possibility of intermediate cell-to-cell signaling steps in wave propagation. Another source is molecular layer interneurons, which can release ATP after parallel fiber stimulation (19).

The unusual symmetry of intercellular waves may arise from the relatively anisotropic properties of extracellular diffusion. For a half life of 200–500 ms (36) the 2-dimensional full-diameter range of ATP is $2^*(4Dt)^{1/2}$ = 25–56 $\mu$m, comparable to the range in 2 dimensions of our observed waves and to observations of ATP spread in cultured astrocytes (3, 11, 37) and ex vivo retinal preparations (38).

The relative contribution of purinergic and gap junction mechanisms to intercellular glial signaling is likely to depend on brain region-specific factors (39). Our observations suggest that in the cerebellum the size of purinergic sources, as well as their rate of clearance and breakdown, allow for local spread of calcium waves to encompass up to dozens of astrocytic processes in vivo. In neocortex, iontophoretic application of ATP can trigger calcium waves that spread beyond the field of view (40), but no evidence has yet been reported from neocortex of spontaneous or synaptically driven ATP-mediated waves. This absence suggests that under many conditions in the intact neocortex, endogenous ATP release events may be relatively small or infrequent. Conversely, gap junction-mediated coupling, a known mechanism for the spread of glial waves in brain slices (39), may be unfavored in cerebellum because gap junction coupling between BG is blocked by calcium itself (41).

**Functional Consequences.** The downstream effects of transglial calcium waves may include blood flow regulation and energetics, neuroprotection, and guidance of synaptic plasticity. Astrocytes are known to play a role in blood flow regulation (30). Activation of molecular layer interneurons can cause vasodilation (42). With ATP release from these cells (19) triggered transglial calcium waves could result in the calcium-dependent release of cyclooxygenases necessary for the local control of blood flow to metabolically active regions. Interestingly, stimulation of the climbing fiber pathway causes lactate accumulation originating from BG, an energy source for metabolically active neurons (43). ATP is also converted to adenosine, which can offer neuroprotection after transient hypoxia (44) and affect synaptic plasticity (45). Thus, known glial and neuronal mechanisms provide several ways in which glial activity can affect brain function. In the cerebellum, the domain-based geometry of ellipsoidal waves suggests that these functions may be organized into groups that are related to one another not just by connectivity, but also by proximity.

## Materials and Methods

**Surgery.** Procedures were performed in accordance with the guidelines of the National Institutes of Health and were approved by local authorities (Princeton University Institutional Animal Care and Use Committee; Cantonal Veterinary Office Zürich). Wistar rats (3–6 weeks) or C57/black6 mice (3–4 weeks) were anesthetized by i.p. injections of either urethane (1.5 g/kg) or a mixture of ketamine (80 mg/kg) and xylazine (6 mg/kg) (Sigma-Aldrich). Body temperature was maintained at 37 °C by using a temperature controller and heating blanket (FHC Inc.). A craniotomy (diameter, 1–2 mm) was made above the crus I or II area of the lateral cerebellum. In rats the dura was removed. Animals anesthetized with ketamine and xylazine were either given supporting doses of anesthetic or kept under anesthesia with 0.5–1.0% isoflurane in oxygen administered by a gas anesthetic regulator (LEI Medical).

**Multicell Bolus Loading of Calcium Indicators.** In vivo bolus loading of indicators was done as described refs. 20 and 21 with an injection depth of the synthetic fluorescent calcium indicators Fluo-5F/AM and OGB-1/AM (Invitrogen) 50–100 $\mu$m below the pia. Agarose (1.0–1.5%, type III-A, Sigma-Aldrich) was dissolved in saline and applied to the brain surface to reduce motion artifacts during imaging.

**Adenovirus with G-CaMP2 and Monomeric DsRed Sequence.** To overcome the low resting fluorescence of G-CaMP2 the monomeric DsRed sequence (Clontech) was inserted at the KpnI site (bp463) of the G-CaMP2 sequence. The resulting fusion sequence (G-CaMP2_DSRed) was inserted into the replication-incompetent adenovirus AdEasy-1 [JHU-23, ATCC (26)] under the CMV immediate-early promoter following the protocol of the AdEasy kit and adenovirus standard procedures (see *SI Methods*).

**Viral Infection with G-CaMP2_DSRed.** A 0.5-mm craniotomy in the crus I or II area of the mouse cerebellum was drilled leaving the dura mater intact; 100–600 nL of virus solution (cell lysate or CsCl purified, 0.2 $\mu$m filtered) was then slowly injected (200–600 nL/h, <0.03 bar) into the brain with a beveled quartz pipette (5-$\mu$m tip opening) at an angle of 45° to the dura and to a depth of ≈200 $\mu$m. After 1–25 days of recovery, craniotomies 1–2 mm wide were made for imaging.

**Two-Photon Laser Scanning Microscopy.** Imaging was performed with custom-built 2-photon microscopes by using CfNT (Max Planck Institut for Medical Research) and ScanImage (46) software. Bolus-loaded tissue was excited at 840 nm by using a Mira 900 (Coherent Inc.) or MaiTai Ti:Sapphire laser (Spectra-Physics)

[†]Nimmerjahn A, Mukamel EA, Schnitzer MJ, Neuroscience 2008, November 15–19, 2008, Washington, DC, abstr 337.2.

focused into the tissue by using a 40×, 0.8 NA (Carl Zeiss or Olympus), or a 20×, 0.95 NA water-immersion objective (Olympus). In tissue expressing G-CaMP2_DsRed, excitation light was 920 nm for calcium imaging and 990 nm for reconstructing morphology. Arbitrary plane calcium imaging (25) in the *x–z* plane was done with the aid of custom-written LabView (National Instruments) software (25) by mounting a 40×, 0.8 NA objective (Olympus) on a piezo-electric fast *z*-focusing device (P-725.4CD, Physik Instrumente) at an excitation wavelength of 870 nm.

**Pharmacology.** For local injections patch pipettes were filled with ATP (1–10 mM, $Na_2$-ATP, Sigma-Aldrich) dissolved in saline containing 135 mM NaCl, 5.4 mM KCl, 1.8 mM $CaCl_2$, 5 mM $MgCl_2$, 5 mM Hepes·HCl, pH 7.3; filtered through a 0.2-$\mu$m pore filter; and positioned in the cerebellar molecular layer. Alexa 594 (15 $\mu$M) was included to visualize the pipette and ATP ejection. Single or brief puff trains (in case of trains 5, 10 Hz puffs of 5–10 ms) were applied at a pressure of $\leq$0.7 bar by using a Pressure System IIe (Toohey Company). PPADS (500 $\mu$M) and suramin (1 mM; both drugs from Tocris) were applied directly to the brain surface.

**Transgenic Animals.** Transgenic mice expressing GFP under the glial fibrillary acidic protein promoter [FVB/N-Tg(GFAPGFP)14Mes/J, stock no. 003257] were obtained from Jackson Laboratories.

**Analysis.** Data were analyzed with custom-written programs in Matlab (Mathworks) and ImageJ (W. S. Rasband, ImageJ, National Institutes of Health, Bethesda, Maryland, http://rsb.info.nih.gov/ij/, 1997–2008).

To identify and quantify regions of spreading calcium change, for all movies $\Delta F/F$ values were calculated for every pixel over the movie duration and thresholded to binary by setting to 1 the pixels $>$2 standard deviations above zero $\Delta F/F$. The ''majority'' morphological operation (MATLAB bwmorph) was applied to each movie frame. This operation was repeated 3 times for all movie frames. Additional mask editing was performed to remove noise that remained. To detect glial waves, the sum $A$ was taken of all ''on'' pixels in a movie frame. The maximum value of $A$ in a movie provided the maximal extent of a wave. Ellipses were fit to the maximum extent of waves by using a stable direct least-square fitting algorithm. Expansion time was defined as the time it took for a wave to reach its maximum extent. Average duration of a wave was defined as the time over which the mean fluorescence change reached 10% of the peak value or greater. Local wavefront velocity (Fig. 1*D*) was calculated by measuring the time for the wave to pass 2 points 10 $\mu$m apart. Average wavefront velocity was calculated by dividing the distance to maximal extent by the duration to maximum extent. A robust linear fit to the rising phase of the 2-dimensional area increase of a wave over time was used to obtain an apparent diffusion coefficient $D_{app}$, where $D_{app} = A/(4*t)$. Data in the text are presented as mean $\pm$ standard deviation unless otherwise stated. Significance tests are one-tailed unless otherwise stated.

**ACKNOWLEDGMENTS.** We thank Jonathan Charlesworth, Peggy Bisher, and Hiroko Nakai for expert technical assistance and Ilker Ozden for helpful comments and critical reading of the manuscript. This work was supported by National Institutes of Health Grant NS045193, the National Science Foundation, the W. M. Keck Foundation, the New Jersey Governor's Council on Autism, the Sutherland Cook fund (S.W.), and a Human Frontier Science Project grant (F.H., J.N., and S.W.).

1. Cornell-Bell AH, Finkbeiner SM, Cooper MS, Smith SJ (1990) Glutamate induces calcium waves in cultured astrocytes: Long-range glial signaling. *Science* 247(4941):470–473.
2. Cotrina ML, *et al.* (1998) Connexins regulate calcium signaling by controlling ATP release. *Proc Natl Acad Sci USA* 95:15735–15740.
3. Guthrie PB, *et al.* (1999) ATP released from astrocytes mediates glial calcium waves. *J Neurosci* 19(2):520–528.
4. Newman EA, Zahs KR (1997) Calcium waves in retinal glial cells. *Science* 275(5301):844–847.
5. Peters O, Schipke CG, Hashimoto Y, Kettenmann H (2003) Different mechanisms promote astrocyte Ca2+ waves and spreading depression in the mouse neocortex. *J Neurosci* 23(30):9888–9896.
6. Nimmerjahn A, Kirchhoff F, Kerr JN, Helmchen F (2004) Sulforhodamine 101 as a specific marker of astroglia in the neocortex in vivo. *Nat Methods* 1(1):31–37.
7. Hirase H, Qian L, Bartho P, Buzsaki G (2004) Calcium dynamics of cortical astrocytic networks in vivo. *PLoS Biol* 2(4):E96.
8. Wang X, *et al.* (2006) Astrocytic Ca2+ signaling evoked by sensory stimulation in vivo. *Nat Neurosci* 9(6):816–823.
9. Schummers J, Yu H, Sur M (2008) Tuned responses of astrocytes and their influence on hemodynamic signals in the visual cortex. *Science* 320(5883):1638–1643.
10. Schipke CG, Haas B, Kettenmann H (2008) Astrocytes discriminate and selectively respond to the activity of a subpopulation of neurons within the barrel cortex. *Cereb Cortex* 18(10):2450–2459.
11. Arcuino G, *et al.* (2002) Intercellular calcium signaling mediated by point-source burst release of ATP. *Proc Natl Acad Sci USA* 99:9840–9845.
12. Weissman TA, Riquelme PA, Ivic L, Flint AC, Kriegstein AR (2004) Calcium waves propagate through radial glial cells and modulate proliferation in the developing neocortex. *Neuron* 43(5):647–661.
13. Chen G, Dunbar RL, Gao W, Ebner TJ (2001) Role of calcium, glutamate neurotransmission, and nitric oxide in spreading acidification and depression in the cerebellar cortex. *J Neurosci* 21(24):9877–9887.
14. Chuquet J, Hollender L, Nimchinsky EA (2007) High-resolution in vivo imaging of the neurovascular unit during spreading depression. *J Neurosci* 27(15):4036–4044.
15. Takano T, *et al.* (2007) Cortical spreading depression causes and coincides with tissue hypoxia. *Nat Neurosci* 10(6):754–762.
16. Kirischuk S, Möller T, Voitenko N, Kettenmann H, Verkhratsky A (1995) ATP-induced cytoplasmic calcium mobilization in Bergmann glial cells. *J Neurosci* 15(12):7861–7871.
17. Kirischuk S, *et al.* (1996) Activation of P2-purino-, alpha 1-adreno and H1-histamine receptors triggers cytoplasmic calcium signalling in cerebellar Purkinje neurons. *Neuroscience* 73(3):643–647.
18. Beierlein M, Regehr WG (2006) Brief bursts of parallel fiber activity trigger calcium signals in bergmann glia. *J Neurosci* 26(26):6958–6967.
19. Piet R, Jahr CE (2007) Glutamatergic and purinergic receptor-mediated calcium transients in Bergmann glial cells. *J Neurosci* 27(15):4027–4035.
20. Stosiek C, Garaschuk O, Holthoff K, Konnerth A (2003) In vivo two-photon calcium imaging of neuronal networks. *Proc Natl Acad Sci USA* 100:7319–7324.
21. Sullivan MR, Nimmerjahn A, Sarkisov DV, Helmchen F, Wang SS-H (2005) In vivo calcium imaging of circuit activity in cerebellar cortex. *J Neurophysiol* 94(2):1636–1644.
22. Reichenbach A, *et al.* (1995) Distribution of Bergmann glial somata and processes: Implications for function. *J Hirnforsch* 36(4):509–517.
23. Charlesworth J (2007) Characterization of acetoxymethyl ester dye loading in the cerebellar molecular layer. Senior thesis (Princeton University, Princeton, NJ).
24. Rice ME, Okada YC, Nicholson C (1993) Anisotropic and heterogeneous diffusion in the turtle cerebellum: Implications for volume transmission. *J Neurophysiol* 70(5):2035–2044.
25. Göbel W, Helmchen F (2007) New angles on neuronal dendrites in vivo. *J Neurophysiol* 98(6):3770–3779.
26. He TC, *et al.* (1998) A simplified system for generating recombinant adenoviruses. *Proc Natl Acad Sci USA* 95:2509–2514.
27. Sato Y, Shiraishi Y, Furuichi T (2004) Cell specificity and efficiency of the Semliki forest virus vector- and adenovirus vector-mediated gene expression in mouse cerebellum. *J Neurosci Methods* 137(1):111–121.
28. Halassa MM, Fellin T, Takano H, Dong JH, Haydon PG (2007) Synaptic islands defined by the territory of a single astrocyte. *J Neurosci* 27(24):6473–6477.
29. Grosche J, *et al.* (1999) Microdomains for neuron-glia interaction: Parallel fiber signaling to Bergmann glial cells. *Nat Neurosci* 2(2):139–143.
30. Takano T, *et al.* (2006) Astrocyte-mediated control of cerebral blood flow. *Nat Neurosci* 9(2):260–267.
31. Tuschick S, *et al.* (1997) Bergmann glial cells in situ express endothelinB receptors linked to cytoplasmic calcium signals. *Cell Calcium* 21(6):409–419.
32. Beierlein M, Regehr WG (2006) Local interneurons regulate synaptic strength by retrograde release of endocannabinoids. *J Neurosci* 26(39):9935–9943.
33. Curtis TM, Scholfield CN (2001) Nifedipine blocks Ca2+ store refilling through a pathway not involving L-type Ca2+ channels in rabbit arteriolar smooth muscle. *J Physiol* 532(Pt 3):609–623.
34. Takata N, Hirase H (2008) Cortical layer 1 and layer 2/3 astrocytes exhibit distinct calcium dynamics in vivo. *PLoS ONE* 3(6):e2525.
35. Klingauf J, Neher E (1997) Modeling buffered Ca2+ diffusion near the membrane: Implications for secretion in neuroendocrine cells. *Biophys J* 72(2 Pt 1):674–690.
36. Dunwiddie TV, Diao L, Proctor WR (1997) Adenine nucleotides undergo rapid, quantitative conversion to adenosine in the extracellular space in rat hippocampus. *J Neurosci* 17(20):7673–7682.
37. Cotrina ML, Lin JH, Nedergaard M (1998) Cytoskeletal assembly and ATP release regulate astrocytic calcium signaling. *J Neurosci* 18(21):8794–8804.
38. Newman EA (2001) Propagation of intercellular calcium waves in retinal astrocytes and Müller cells. *J Neurosci* 21(7):2215–2223.
39. Haas B, *et al.* (2006) Activity-dependent ATP-waves in the mouse neocortex are independent from astrocytic calcium waves. *Cereb Cortex* 16(2):237–246.
40. Tian GF, *et al.* (2005) An astrocytic basis of epilepsy. *Nature Med* 11(9):973–981.
41. Müller T, Möller T, Neuhaus J, Kettenmann H (1996) Electrical coupling among Bergmann glial cells and its modulation by glutamate receptor activation. *Glia* 17(4):274–284.
42. Rancillac A, *et al.* (2006) Glutamatergic Control of microvascular tone by distinct GABA neurons in the cerebellum. *J Neurosci* 26(26):6997–7006.
43. Caesar K, *et al.* (2008) Glutamate receptor-dependent increments in lactate, glucose and oxygen metabolism evoked in rat cerebellum in vivo. *J Physiol* 586(5):1337–1349.
44. Lin JH, *et al.* (2008) A central role of connexin 43 in hypoxic preconditioning. *J Neurosci* 28(3):681–695.
45. Pascual O, *et al.* (2005) Astrocytic purinergic signaling coordinates synaptic networks. *Science* 310(5745):113–116.
46. Pologruto TA, Sabatini BL, Svoboda K (2003) ScanImage: Flexible software for operating laser scanning microscopes. *Biomed Eng* 2:13.